Structure and Morphology of Model Polymer Electrolyte Membranes Based on Sulfonated Syndiotactic-Polystyrene in the δ Co-Crystalline Phase Resolved by Small-Angle Neutron Scattering

M. M. Schiavone[1], O. Tarallo[2], R. Di Girolamo[2], L. Caporaso[3], M-S. Appavou[1], Z. Revay[4], and A. Radulescu[1*]

[1]Jülich Centre for Neutron Science (JCNS) at Heinz-Maier Leibnitz Zentrum (MLZ), Forschungszentrum Jülich GmbH, Garching, Germany

[2]Dipartimento di Scienze Chimiche, Universita' degli Studi di Napoli Federico II, Italy

[3]Dipartimento di Chimica e Biologia, Universita' degli Studi di Salerno, Italy

[4]Technische Universität München, Forschungsneutronenquelle Heinz Maier-Leibnitz FRM II, Garching, Germany

* corresponding author: a.radulescu@fz-juelich.de

Abstract Syndiotactic polystyrene (s-PS) is able to form different kinds of co-crystalline phases with guest molecules of different size, shape and property. Several advanced materials have been produced starting from s-PS co-crystalline films. In particular, sulfonated s-PS (s-sPS) can be used as proton-conductive membrane in some fuel cells applications, as it presents high proton conductivity (comparable with Nafion). Besides, it shows a high chemical and thermo-mechanical stability and a low cost. The morphology of different s-PS clathrates and the structural behavior of s-sPS upon hydration can be thoroughly understood by SANS. In fact, exploiting the neutron contrast variation between various hydrogenated and deuterated components of s-PS and s-sPS clathrates, additional and unique information about the distribution of guest molecules in the crystalline and amorphous regions and about the hydrated domains of the polymer were obtained. Moreover, using uni-axially deformed films the occurrence and distribution of scattering features from typical morphologies on specific directions and sectors of detection plan enable an accurate structural study of such complex polymeric systems. We report in the present paper a detailed SANS investigation of s-PS films, starting from their crystallization with guest molecules to the subsequent sulfonation and hydration. FT-IR, neutron PGAA, WAXD and cryo-TEM were used complementary to SANS to check the state of the samples after each step of the treatment process and to obtain additional structural information as support for the understanding of the SANS data. The current experimental analysis has highlighted that the morphology of these polymeric films is characterized by hydrated channels in the bulk amorphous phase alternated to stacks of crystalline lamellae, oriented along the stretching direction.

Keywords: sulfonated syndiotactic polystyrene, δ co-crystalline phase, PEM, SANS.

1. Introduction

Polymer Electrolyte Membranes (PEMs, also called proton exchange membranes) are typically ionomers of interest for applications such as fuel cells [1], solar energy conversion devices [2] and water filtration [3]. PEM for fuel cells (PEMFC) [4] are considered today as one of the most promising technologies in the field of renewable power sources and environmentally friendly energy generation, to solve the problems of oil shortage and global warming due to their high efficiency and the clean exhausts [5]. To be considered a good candidate as membrane for fuel cell applications, specially designed polymers and copolymers have to present different properties, such as: high ionic conductivity, resistance to dehydration, adequate mechanical strength, chemical and electrochemical stability under operating conditions, low gas permeability, moisture control in stack, low cost production and good capability for fabrication into membrane electrode assemblies. Currently, the most used material for such applications is the Nafion (N115, N117 and N1110, chemically stabilized perfluorosulfonic acid/polytetrafluoroethylene [PFSA/PTFE] copolymers in the acid (H^+) form), produced for the first time in the 1970s by Du Pont^{TM}. However, despite the excellent properties of the Nafion membranes, there are several disadvantages such as the high cost, the lack of safety during its manufacture and use, requirement of supporting equipment and temperature related limitations [4-8]. Moreover, under the more stringent operating conditions requested by industry (T>100 °C and RH<50 %), proton conductivity for PFSA membranes drops significantly, leading to a decrease in fuel cell performance [9]. This has prompted the research towards the analysis of alternative polymers that could be used as PEMFCs. In this regard, non-fluorinated membranes with aromatic backbone, non-fluorinated hydrocarbons, acid-base blends and partially sulfonated polymers have become the subject of numerous scientific investigations in the industry and academic world [4, 6-8, 10]. Recently some authors [11-14] have proposed a proton-conductive membrane based on sulfonated syndiotactic polystyrene (s-sPS), which presents a high proton conductivity, high chemical and thermo-mechanical stability and a low cost. Moreover, its thermoplastic nature allows for easy processing in forms suitable for several applications, like films, membranes, and foams, as well as their recycling. At the same time, the very complex polymorphic behavior and the extreme sensitivity to the processing conditions spurred many investigations on it [15].

The sPS can crystallize in many crystal forms as well non-equilibrium structures depending on the thermo-mechanical processing conditions [16-22]. The most stable α and β forms are characterized by chains in *trans*-planar (zig-zag) conformation and principally obtained by melt crystallization or by annealing at the appropriate temperature, whereas the γ form [23] is characterized by chains in helical conformation and can be prepared through solvent treatments of the amorphous phases or α form followed by annealing at high temperatures. Two nanoporous crystalline phase, called δ [23-25] and ε [26-32], have been discovered for this polymer (with the same helical conformation *s(2/1)2* of the γ form), which can absorb several guest molecules so producing clathrate and intercalate co-crystals [29-32]. In particular, different advanced materials [33-35] have been already produced starting from s-PS co-crystalline films.

As previously mentioned, a field in which sPS may be employed is that of PEMs, once appropriately functionalized [36-37]. However, a number of issues related to the practical use of the sulfonated hydrocarbon polymer PEMs in fuel cell applications were reported in various publications. Thus, a strong reduction of the sPS crystallinity as a consequence of sulfonation procedure in solution was observed [38, 39]. Another problem is related to the durability of the sPS PEMs. Several studies reported degradation of polystyrene based membranes at high temperatures, due to their oxidation decomposition in practical fuel cell systems conditions [40-42]. Anyway, recent developments have shown that, at least at the laboratory scale, these problems can be successfully tackled. In their study, Fasano et al. [14] have set up a method of using a bulky sulfonating agent which, when applied to δ form sPS samples, leads to an efficient and uniform phenyl ring sulfonation only in the amorphous phase, without disturbing the polymer crystallinity. Such membranes were prepared and characterized from a macroscopic point of view and a value of proton conductivity of 10^{-3} to 10^{-2} S/cm, comparable with that exhibited by Nafion membranes [4,13-14], was reported. On the other hand, Saga et al. [43] prepared composite polyelectrolyte membranes from sulfonated polystyrene and fullerenes and concluded that the addition of fullerenes improved the oxidation resistance of the membranes due to the radical scavenging role played by the fullerenes. More recently, aiming to increase the operating temperature of Li-ion batteries (LIB), Raut et al. [44] fabricated and characterized sPS ionogel membranes for use in such applications. The membranes were found to be stable over a long time in high temperature electrochemical operations, such in LIBs.

It is generally accepted that the properties of PEMs derive from the microphase separation of a hydrophilic ionic material from a hydrophobic substance. Therefore, to design new PEMs, one should not only consider the architecture of the molecule itself, but also understand the microphase separation structures of membranes, such as the crystalline domains, the formation of conducting regions, and the distribution of ionic groups and water in the conducting regions. Even the microstructure of the Nafion is still debatable, as shown by the continuous interest raised by this material regarding the microstructural investigations by small-angle scattering techniques, either X-ray (SAXS) or neutrons (SANS). Several morphologies involved in the microstructural conduction mechanisms were proposed for Nafion along the time: from Gierke's model of inverted-micelle water clusters [45-48], through layered structures [49, 50], channel networks [45, 51, 52], polymer bundles [53-55], parallel randomly packed water channels [56] until the most recently proposed flat and narrow water domains yielding "water films" [57]. A comprehensive summary of PSFAs, including Nafion, with a detailed description of their nanomorphology and transport properties is reported in [58].

In this paper we report a detailed microstructural characterization of membranes based on sulfonated syndiotactic polystyrene (s-sPS) in the δ-clathrate co-crystalline phases carried out by using primarily SANS with contrast variation. The investigation on the structural behavior of s-sPS films was done upon their clathration, sulfonation and subsequent hydration either by dipping in water or by exposing them to controlled relative humidity (RH) by means of a humidity chamber (Anton Paar). Complementary techniques like FT-IR spectroscopy, neutrons prompt gamma activation analysis (PGAA), wide angle X-ray scattering (WAXS) and transmission electron microscopy using the cryo option (cryo-TEM) were used before or after film hydration to enable a complete system characterization prior to SANS investigations or as

support for the interpretation of the SANS observations. Neutron contrast variation was used to emphasize or to mask different regions of the complex s-sPS system. By clathration, crystalline regions showing cages that are filled with certain guest molecules were generated in the sPS films as dispersed in an otherwise amorphous phase. The crystalline region itself consists of crystalline lamellae alternating with amorphous inter-lamellar regions. The reported crystallinity of such sPS samples was about 40% [59]. Therefore, the neutron contrast between the crystalline and amorphous regions can be varied by loading either hydrogenated or deuterated guest molecules into the crystalline regions [60]. The sulfonation of sPS films affects exclusively the amorphous regions, which can thus change further the neutron contrast between the amorphous and crystalline regions. Furthermore, exploring the hydration of the samples for different D_2O/H_2O ratios, we aimed for another contrast manipulation between the crystalline and amorphous regions. Particular interest was focused on the investigation whether the hydration will affect both the inter-lamellar and bulk amorphous regions or only the bulk amorphous region of the system.

Finally, in order to be able to analyse better all scattering features yielded by such a complex system we used uni-axially deformed (oriented) sPS films to separate the scattering signals from different regions of the film morphology on different sectors of the two-dimensional position sensitive detector used for SANS [59]. A schematic design of the SANS investigation geometry is shown in Fig. 1. Following this experimental approach we were able to characterize in details the complex morphology of s-sPS films in dry or hydrated state and to evidence the water one-dimensional regions, which possibly emerge at a later stage by linking together initially formed water clusters in the bulk amorphous region of the films.

2. Experimental Part

2.1 Synthesis

The deuterated syndiotactic polystyrene (d_8-sPS) sample was prepared using the homogeneous catalytic system composed of pentamethylcyclopentadienyltitanium trichloride (Cp^*TiCl_3) and methylalumoxane (MAO) in toluene. All manipulations of air- and/or water-sensitive compounds were carried out under dry nitrogen atmosphere using a Braun Labmaster drybox or standard Schlenk line techniques. Glassware and vials used in the polymerization were dried in an oven at 120°C overnight and exposed to vacuum-nitrogen cycle, three times.

d_8-Styrene (Aldrich, isotopic purity 98% atom% D) was purified by distillation under reduced pressure over CaH_2. Cp^*TiCl_3 was purchased from Stream and used as received. MAO was purchased from Chemtura. Toluene was refluxed 48 h over metallic sodium and distilled under a nitrogen atmosphere.

The polymerization run was carried out in a 250 mL glass flask provided with a magnetic stirrer and thermostated at 40 °C in an oil bath. The reactor was charged under nitrogen sequentially with toluene (7 mL), dried MAO ($14 \cdot 10^{-3}$ mol), and styrene-d_8 (28 mL). A solution obtained by dissolving Cp^*TiCl_3 ($5.4 \cdot 10^{-3}$ g) in toluene (3mL) was then added to the reactor via syringe to

initiate the polymerization. The polymerization was stopped after 12 h by injecting acidified methanol.

The polymer was recovered by filtration, washed with fresh methanol, and dried in vacuo at 60 °C. The yield was 3.5 g. The polymer fraction insoluble in methyl-ethyl-ketone was 95%.

Molecular weights (M_w and M_n) and polydispersity (M_w/M_n) were determined by high temperature gel permeation chromatography (GPC). All analyses were performed with a Waters Alliance 2000 liquid chromatograph. The GPC columns were eluted with 1,2,4-trichlorobenzene (TBC) at 140°C at 1.0 mL/min and were calibrated using monodisperse polystyrene standards. The deuterated syndiotactic polystyrene used in this work presents a weight-average molar mass M_w of 822,300 g/mol with a dispersity index M_w/M_n = 1.63.

2.2 Sample preparation

All the protonated and deuterated solvents used for the preparation of the samples (chloroform, dodecanoic acid, chlorosulfonic acid and acetone) were purchased from *Sigma-Aldrich* and used without any further purification. Even the deuterated solvents purchased from *Armar Chemicals* were used as received.

Uni-axially oriented δ-clathrate *d8*-sPS/toluene samples were obtained by exposure of oriented samples in the α-phase to toluene at room temperature for one week, keeping fixed the ends of the specimen. Fibers of the α-form were obtained by drawing un-oriented α-form samples, stretching twice on a hot plate at a temperature in the range 105-110°C. Un-oriented α-form specimens were prepared in a hot press by melting at 270 °C and successive rapid cooling in a bath of water and ice. Un-oriented δ-form clathrate samples have been obtained by casting a polymer-chloroform solution onto a glass substrate to form a film. The solution was prepared at 2 wt % and then heating up to about 70°C for 1 hour until complete polymer dissolution. The solution was subsequently poured into a Petri's dish, so allowing the partial evaporation of the solvent and the obtainment of the cast film directly in the δ co-crystalline form with $CHCl_3$ as guest molecule. The thickness of the cast and drawn films was about 50-100 μm.

The deuterated s-PS films was functionalized using as sulfonation reagent a solution of 0.2M acyl sulfate in deuterated chloroform, soaking films directly in the prepared solution for 2h at about 50 °C, adopting a procedure similar to that one reported in [61]. Afterwards, the samples were removed from the solution and quickly dipped in acetone for few minutes to remove traces of impurities (due to the possible remnants of the sulfonation procedures) and dried to the air under the fume-hood for 24 h. The acyl sulfate was prepared by mixing at room temperature a molar ratio (1:1) of dodecanoic acid and chlorosulfonic acid under nitrogen atmosphere for a time of 24 h. Acyl sulfate, despite its toxicity, is preferred to other, mostly more efficient sulfonating agents (such as SO_3, SO_3 in H_2SO_4, chlorosulfuric acid) mainly because it practically does not cause degradation of the polymer chain and does not lead to the sulfone formation and hence to crosslinking [62].

The s-sPS films were subsequently subjected to guest exchange procedure [60] to exchange the chloroform and acetone guest molecules trapped in the cages between the sPS helices with other kind of molecules, in a controlled way. Deuterated toluene (d-Tol) or protonaned toluene (h-Tol) were loaded by dipping the films in solvents for about 1 day, to vary the neutron scattering length density (SLD) of the crystalline regions and to enable variation of the neutron contrast between the amorphous and crystalline domains of the samples. Further on, selected samples were hydrated by direct immersion in solutions of H_2O and D_2O at different ratios. The hydration affected only the amorphous regions of the samples, varying further the neutron scattering contrast between different regions of the samples.

2.3 Fourier-Transformed Infrared Spectrometry (FTIR)

The qualitative and quantitative analysis of the degree of sulfonation of the samples was checked by FTIR and neutrons PGAA. FTIR spectra were obtained at a resolution of 2.0 cm^{-1} with a PerkinElmer (Spectrum Two) spectrometer equipped with a deuterated triglycine sulfate detector and a Ge/KBr beam splitter. The frequency scale was internally calibrated to 0.01 cm^{-1} using a He-Ne laser. The scanned wavenumber range was 4000-400 cm^{-1}. 32 scans were signal averaged to reduce the noise. The thickness of films used was always about 50 μm, in order to keep peaks of interest in the range of absorbance-concentration linearity.

2.4 Neutron Prompt-Gamma Activation Analysis (PGAA)

Neutron PGAA measurements were carried out at the PGAA neutron instrument of Heinz Maier-Leibnitz Zentrum (MLZ) in Garching (Germany) [63]. The neutron beam size was 11 × 16 mm^2, which delivered a maximum neutron flux on the sample of 4×10^{10} cm^{-2} s^{-1} (thermal equivalent). A Compton-suppressed spectrometer (60% HPGe detector surrounded by a BGO scintillator and connected in anticoincidence mode) was used to detect the gamma radiation. The signals were processed using a Canberra DSPEC-50 digital spectrometer. The energy range of the spectra was 50 keV–11600 keV. The experiments were made in a low vacuum of 0.3 mbar.

2.5 Ionic Exchange Capacity

The Ionic Exchange Capacity (IEC) was calculated adopting a procedure described in [64]: every sample (~10 mg) was dipped overnight at room temperature in 1.2 M hydrochloric acid to ensure protonation of all the sulfonic acid groups. Successively, s-sPS films were washed with deionized water many times to remove completely any traces of acidic solutions. Afterwards they were ion-exchanged in 20 mL 0.1 M NaCl by soaking for 2 days. The pH value of the proton-exchanged NaCl solution was measured using a pH meter (Mettler Toledo Seven Compact) and the IEC [meq/g] was determined using the following equation

241 $IEC = (10^{-pH} \times V_{NaCl})/m_0$ (1)

242 where V_{NaCl} (in l) is the volume of NaCl solution and m_0 (in g) is the dry mass of the membrane.

243

244 **2.6 Water Up-Take**

245 At first, s-sPS films were dried in a vacuum oven for three nights at 40 °C, and then they were
246 equilibrated in deionized water for 24 h and blotted with a Kimwipe to remove surface water
247 prior to determining the 'wet' weight. The water up-take was calculated as the percentage
248 increase in mass over the "dry" weight as following:

249 Water up-take $= [(W_{wet}-W_{dry})/W_{dry}]\times 100\%$ (2)

250 where W_{wet} and W_{dry} are the wet and dry weight of the membrane, respectively.

251 The water content was calculated as a mass percentage of the water in the "wet" membrane and
252 given by:

253 Water content (wt %) $= [(W_{wet}-W_{dry})/W_{wet}]\times 100\%$ (3)

254 IEC, water up-take and water content were taken as the average values of at least three
255 membrane samples.

256

257 **2.7 Wide-Angle X-rays Diffraction (WAXD)**

258 The X-rays fiber diffraction patterns of oriented samples were obtained on a BAS-MS imaging
259 plate (FUJIFILM) with a cylindrical camera (radius 57.3 mm, Ni-filtered Cu-Kα radiation) and
260 processed with a digital scanner. Clathrated and sulfonated s-sPS films were controlled with
261 this method. Later checks of films prior or after hydration and drying were done by rapid scan
262 in the range of 2θ 5°-35° through a X-Ray Powder diffractometer Brucker 2nd Gen- D2 Phaser
263 (Cu-source).

264

265 **2.8 Transmission Electron Microscopy (TEM)**

266 Sections of hydrated s-sPS film were produced by using a Leica FC7 cryo-ultra-microtome.
267 The sections were obtained from the transversal orientation perpendicular to the streching
268 direction. The cryo-sectionning was performed at -35°C in liquid nitrogen atmosphere, i.e.
269 below the T_g of sPS, with the aim to harder the specimen block enough for the sectioning. The
270 specimen was cryo-fixed by rapid immersing into liquid nitrogen then inserted into a Multi-
271 Specimen Cryo Transfer Holder (Model 910, Gatan, Munich, Germany) and transferred to a
272 JEM 2200 FS EFTEM instrument (JEOL, Tokyo, Japan). Examinations were carried out at
273 temperatures around -180°C. Images have been taken with EMenu 4.0 image acquisition
274 program (TVIPS, Munich, Germany) and processed with a free digital imaging processing
275 system Image J [65].

2.9 Small-Angle Neutron Scattering (SANS)

All SANS experiments on un-oriented (cast) and oriented (uni-axially deformed) samples were carried out at the KWS-2 SANS diffractometer of the JCNS at Heinz Maier-Leibnitz Zentrum (MLZ) in Garching, Germany [66]. A neutron wavelength λ=5 Å with a spread of $\Delta\lambda/\lambda$ = 20% was used for all SANS investigations. The data were collected at different sample-to-detector distances, typically 2, 8 and 20 m. Detection distances of 1 m and 4 m were involved in some cases when special scattering features appeared in specific Q ranges. The data acquisition was done on two different detectors, because the microstructural investigation on different s-sPS systems spread over a period of time coinciding with the upgrade of the detection system at KWS-2 diffractometer. In the first part of the study a scintillation detector with an active area of 60 cm x 60 cm and a resolution of ca. 7.5 mm was used while later SANS experiments involved a ^{3}He tubes array detector with an active area of about 0.9 m^2 and a resolution of 8 mm [66]. The deuterated sPS and s-sPS membranes were investigated in different states. First, dry un-oriented and oriented samples were characterized using a beam-size of 6 x 8 mm^2. Hydrated s-sPS films obtained by dipping over the night in water at different D_2O/H_2O ratios were tightly closed in sandwich type cells with quartz widows (Hellma Analytics) and measured by using a similar beam size. Samples exposed to gradual hydration-drying processes were measured at different relative humidity (RH) values by using an Anton-Paar humidity chamber installed at the sample position of the SANS diffractometer. The humidity cell (Figure supplementary material) provided controlled RH and temperature on the sample and enabled measurement of sample by using a neutron beam size that was defined by a circular Cd aperture with a diameter of 4 mm. For all types of systems, several samples were investigated by SANS in similar conditions, to confirm the experimental observations.

The two-dimensional scattering data were corrected for the detector sensitivity, instrument noise and scattering from the empty cell and subsequently calibrated in absolute units by using the Plexiglas standard sample at the instrument. Data from un-oriented samples were subsequently radially averaged to obtain the one dimensional $I_1(Q)$. Scattering patterns from oriented samples were averaged over narrow angular sectors along the meridian and equatorial directions to deliver the $I_1^{eq}(Q)$ and $I_1^{m}(Q)$ that contain information about the oriented and aligned morphologies in the sample due to stretching.

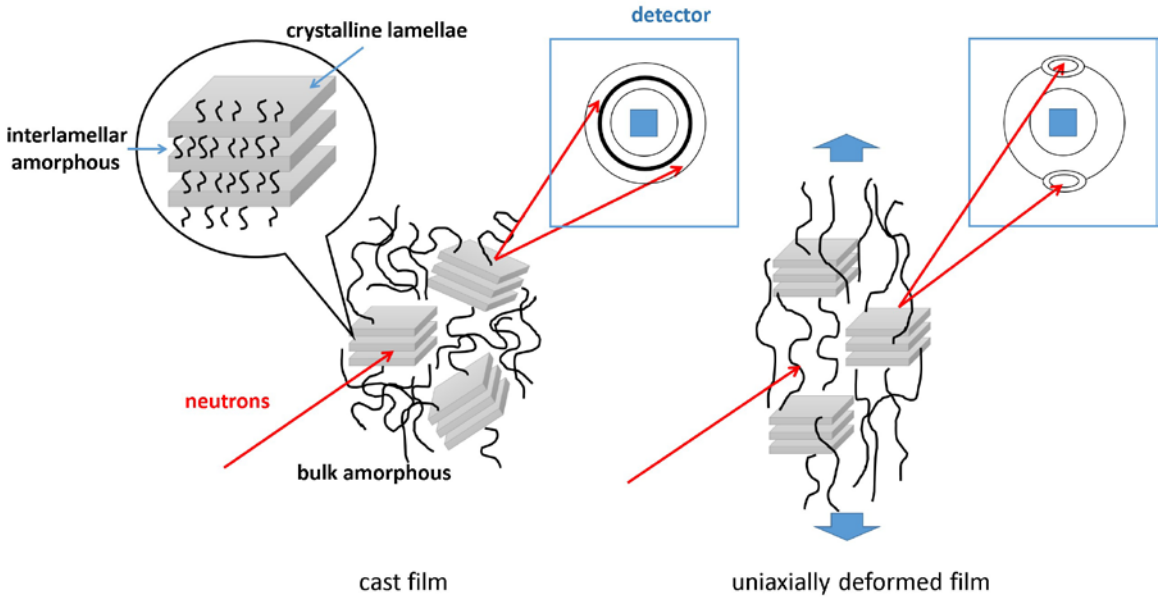

Fig.1 – Schematic view of the experimental SANS approaches used for the investigation of the s-sPS films: left – cast films consisting of randomly oriented lamellar stacks and bulk amorphous regions; the cast films produced isotropic scattering patterns on the two-dimensional position sensitive detector; right – uni-axially deformed films which produce on the detector clearly separated inter-lamellar peaks due to orientation of the lamellar stacks along the deformation axis. The lamellar stacks contain crystalline lamellae and inter-lamellar amorphous domains.

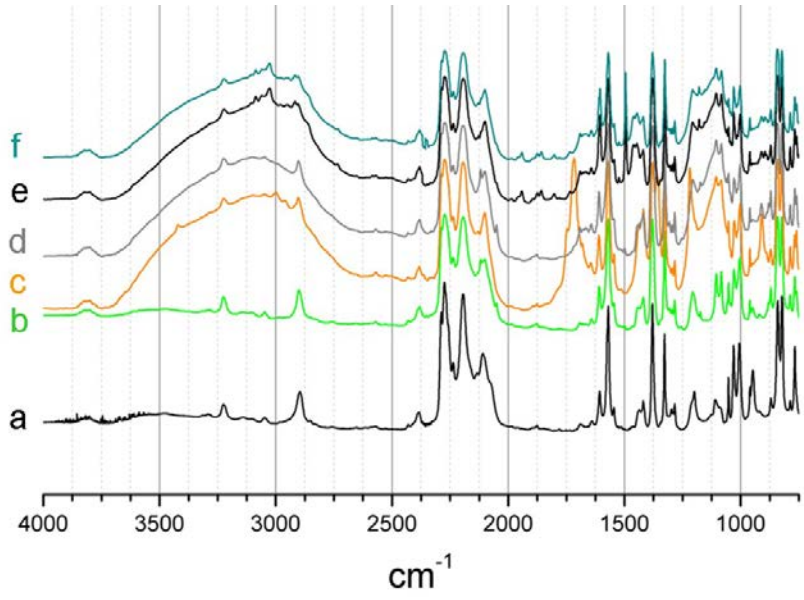

Fig. 2 – FTIR spectra from sPS films after each step of the preparation and functionalization procedure: a – sPS film as prepared (α-form); b – clathrate film with d-Tol; c – sulfonated film in a chloroform-based acyl sulfate solution; d – clathrate and sulfonated film containing d-Tol after guest exchange procedure (replaced the chloroform); e – sPS film after the guest exchange procedure between d-Tol and h-Tol; f – same film as for the curve e, after it was kept in oven at 40°C under vacuum for 60 minutes.

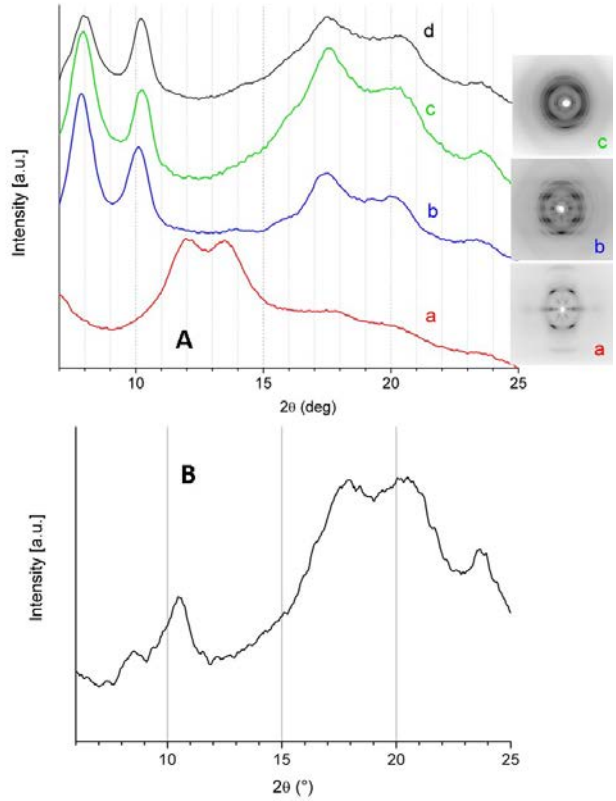

Fig. 3 – top (A): WAXD patterns (two-dimensional and one-dimensional after averaging over the equatorial sectors) from uni-axially deformed sPS films; a: sPS film as prepared (α-form); b: clathrate film (δ phase); c: sulfonated film (δ phase); d: film after the guest exchange (with d-Tol); bottom (B): WAXD pattern (one-dimensional scan) from a s-sPS film which was dried after exposed to hydration procedure using the humidity chamber.

3. Results and discussion

FT-IR spectra for an oriented deuterated s-sPS film at different stages of the preparation procedure are presented in Fig. 2. The spectra were collected on the initial α-phase (curve a), following then the clathration with d-Tol and formation of the δ-clathrate (curve b), sulfonation using chloroform based solution (curve c), guest exchange between the chloroform and d-Tol (curve d), up to finally the guest exchange between d-Tol and h-Tol (curve e). The final stage (curve f) was achieved after drying the film at 40°C under vacuum for 60 minutes, in order to remove all residues from the amorphous regions. The identification of the sulfonic acid IR bands is quite difficult, because some bands of absorbance from deuterated polystyrene are overlapping with those from sulfonic acid. However, the two very broad bands shown by the curves c-f in the wavenumber range of 2500-3700 cm^{-1} and 1000-1300 cm^{-1} are indicative for the sulfonation of the sample. Most likely the large band between 1000 and1300 cm^{-1} is a convolution of several absorption bands (such as that one expected for the s-sPS at 1127 cm^{-1}, relative to the in-plane skeletal stretching vibration of the di-substituted aromatic ring and at 1176 cm^{-1} due to the asymmetrical stretching vibration of the sulfonic group [67]). Additionally, the stretching vibration ν_{as} (SO_2) of $R–SO_3^-$ compounds generally shows a strong and broad

band typically in the range 1250-1150 cm^{-1} [68]. As for the observed peaks at 1083 and 1053 cm^{-1}, they can be assigned to vibrations of the deuterated main chain of the polymer [69]. Nevertheless, the sulfonation of the polymer was definitely confirmed via the peak centered at 1104 cm^{-1}, corresponding to the in-plane bending vibration of the benzene ring substituted by $–SO_3H$ [70, 71].

The tracks of acetone and chloroform used during the sulfonation procedure can be observed in the range 1250-1750 cm^{-1}. These features are not anymore shown by the curves d-e, which proves the success of the guest exchange procedure subsequently applied to the sulfonation one. Finally, the presence of the new line slightly below 1500 cm^{-1} in the curves e and f indicates the presence of h-Tol as guest molecule in the crystalline cages of the sPS, which exchanged the d-Tol molecule present in the previous stage (curve d).

From the quantitative point of view, PGAA analysis also confirmed the successful sulfonation reaction. A sulfonation degree of about 40 % for the un-stretched samples and of about 60 % for the stretched ones was determined by using the method reported in [72]. Unlike the extent of sulfonation, which could be controlled, the locations of the sulfonic acid groups could not be determined. It is thus expected that the sulfonic acid groups are randomly distributed within the amorphous phase, similarly as was observed in other cases [14, 61, 72].

The results obtained from the analysis of the water uptake and ionic exchange capacity (Table 1) show that the s-sPS films which have been produced present similar properties with those reported in the literature and may be considered model systems of materials which can potentially be used in PEM applications.

Fig. 3a present WAXS results collected on s-PS films at different stages along the preparatory process including production of drawn samples (curve a), clathration of the crystalline regions (curve b) and sulfonation (curve c). The pair of the sharp peaks shown by curves b and c at around 8° and 10° in 2θ are indicative for the formation and preservation of the δ-crystalline phase of clathrates after the treatment of the films along the preparation process [73]. Moreover, dried films after their hydration and investigation by SANS exhibit the same patterns (Fig. 3b). This is a strong indication that the δ-crystalline phase of the sPS system is preserved even after chemical and humidity treatment of films, which is consequently a first proof of the mechanical strength of the system, an appropriate property requested in PEM applications.

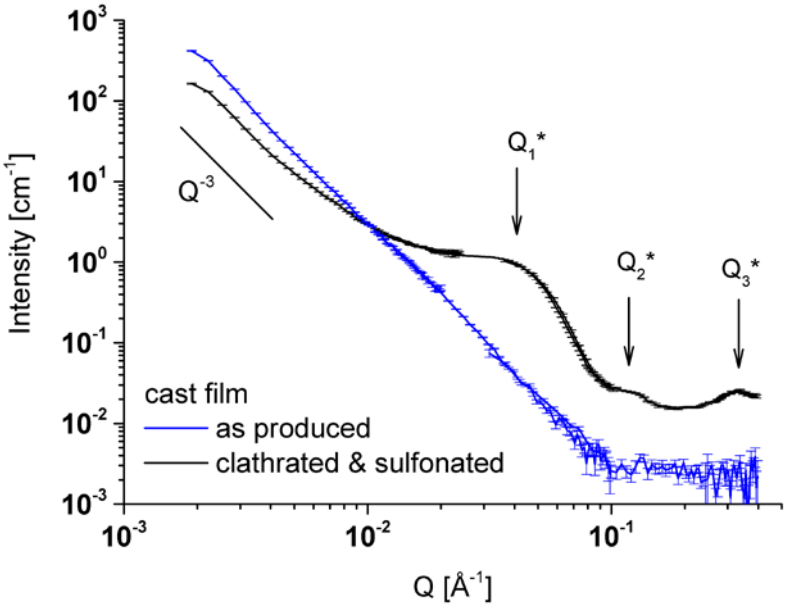

Fig. 4 – One-dimensional SANS patterns from cast films as produced and after clathration and sulfonation. The power law behavior of the scattering at low Q and the observed maxima are indicated.

3.1 SANS on cast films

SANS results obtained on a cast film in a dry state are shown in Fig. 4.

Typically, the SANS and SAXS spectra from Nafion or other semi-crystalline ionomers display distinct features in three Q-regimes from which structural information is obtained [58, 74]: i) the small Q-regime, where there is typically an upturn due to the large scale structural features of the polymer film; ii) a intermediate Q-regime between 0.01 and 0.1 Å^{-1} where a broad feature corresponding to inter-crystalline spacing ("matrix knee") appears and iii) the high Q-regime (around 0.1-0.5 Å^{-1}) where the most characteristic feature is observed, namely the ionomer peak due to correlation spacing between the hydrophilic water domains. A comprehensive description of the characteristic scattering features from perfluorinated sulfonic-acid ionomers can be found in the review of Kusoglu and Weber [58].

Towards higher Q values a so-called "SO_3" peak characteristic of the distance between sulfonated units along the rigid polymer backbone can be observed in some cases [75]. At very high Q, typically out of the SANS/SAXS domain, the amorphous and crystalline peaks may be observed, corresponding to the inter- and intra-crystalline spacing. The ionomer peak grows and shifts towards lower Q values during humidification of membrane while the "SO_3" peak remains stable or shifts towards higher Q values [75].

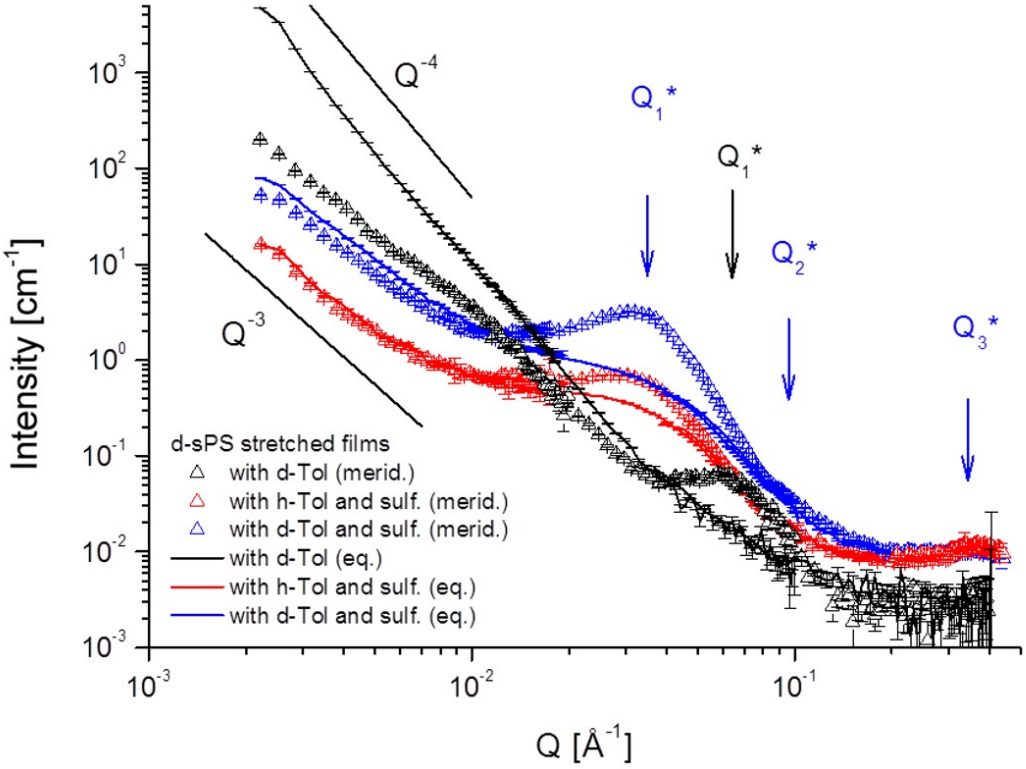

401

402 Fig. 5 – One-dimensional SANS patterns from uni-axially deformed films after clathration and
403 sulfonation (both meridian and equatorial sectors). The films were placed with the stretching direction
404 vertically in beam.

405

406 The sPS cast film shows a typical monotonous increase of the scattered intensity towards low
407 Q with a Q^{-p} power low behavior with exponent *p* between 3 and 4, as expected from systems
408 dominated by surface fractals and roughness features [76]. Although the film is clathrate, no
409 feature due to possible inter-lamellar correlations in the crystalline regions is observed, which
410 may be explained by the weakening of such effects due to the random character of the films
411 obtained by casting (Fig. 1).

412 Sulfonated cast films display a scattering pattern revealing several striking scattering features:
413 the clear peak at around Q=0.35 Å^{-1}, the hump observed at around Q=0.12 Å^{-1} and the broad
414 and prominent feature observed at around Q=0.03-0.05 Å^{-1}. Although intuitively the high Q
415 peak (Q_3*) may be considered the ionomer peak, which was previously observed in the SAXS
416 patterns on s-sPS systems [13], and the broad hump (Q_1*) occurs at Q values where typically
417 the "matrix knee" is observed, the exact nature of these features is difficult to straightforwardly
418 explain in an unambiguous way by only analyzing the cast films, without further treatment of
419 samples. Based on the processes applied to the sPS films during their production and treatment,
420 it is expected that different morphologies and microscopic correlation effects would contribute
421 in a combined way to the occurrence of such features.

422

423

3.2 SANS on uni-axially deformed films

SANS investigation of uni-axially deformed (stretched) films helped for disentanglement of such complex morphologies (Fig. 1). Fig. 5 shows the scattering patterns from stretched clathrate and subsequently sulfonated films. The guest molecules in the crystalline regions (clathrates) have been exchanged to either deuterated (d-Tol) or protonated (h-Tol) species of the same molecule (toluene) *via* dipping the films in the corresponding solutions. The data were separately analyzed on equatorial and meridian sectors of the anisotropic 2D scattering patterns (Figs. 6b and 6c).

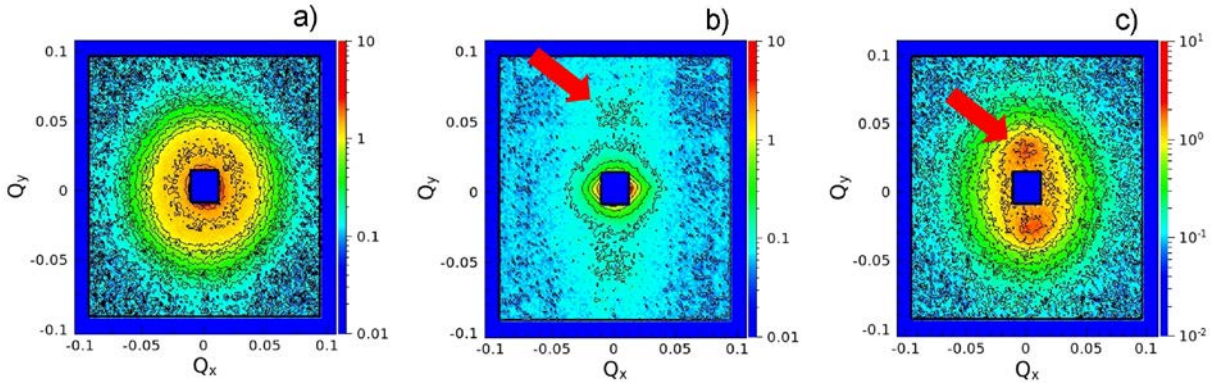

Fig. 6 – Two-dimensional scattering patterns from a sulfonated cast film (a) and a uni-axially deformed film after the clathration (b) and sulfonation (c) procedures. The data were collected at a detection distance of 4 m after the sample. The stretching direction of the uni-axially deformed films was vertical; the arrows indicate the position of the peaks which appear in meridian sectors due to the inter-lamellar correlations: the peaks shift towards the beam stop (lower Q values) when the film is sulfonated.

The scattering pattern from the clathrate film displays a striking feature that appears clearly as a peak in the meridian sectors at around Q=0.065 $Å^{-1}$. This feature is likely due to inter-lamellar correlations between the vertically aligned crystalline lamellae because of the uni-axial film deformation (Fig. 6b) as schematically depicted in Fig. 1. In this example, the contrast appears between the crystalline lamellae and the amorphous inter-lamellar regions (Fig. 1) due to the difference in polymer density (Table 1), on one hand, and the presence of guest molecules in the crystalline lamellae, on the other hand [59, 60]. The analysis of similar data *via* one-dimensional correlation function derived from the scattered intensity was performed using a procedure like that presented in [77], and delivered an inter-lamellar spacing of about L_D=100 Å [59].

Sulfonation results in the formation of a very complex morphology. All one-dimensional scattering patterns from clathrate and sulfonated uni-axially deformed films (Fig. 5) show in principle the same three features as those shown by the cast films. The nature of these features is understood following the deformation of the film and thus, the separation of different scattering contributions over meridian and equatorial sectors. From the parallel examination of the two-dimensional scattering patterns from un-oriented (Fig. 6a) and oriented (Fig. 6c) samples it can be presumed that the Q_1* feature in the one-dimensional scattering pattern in

Fig. 4 represents a superposition of two contributions, which are clearly evidenced in the one-dimensional scattering patterns separately averaged over the meridian and equatorial sectors reported in Fig. 5.

On one hand, clear peaks due to correlations between oriented morphologies are observed in the meridian sectors (Fig. 6c). The peaks appear at lower Q values as in the case of the film that was only clathrate (Figs. 6b abd 6c). Taking into account the complementary information delivered by WAXS, namely the presence of the δ-crystalline phase, and by FTIR, namely that the toluene molecules are still present in the sample as guests in the cavities of the δ-crystalline phase, the peaks can be ascribe further to correlations occurring between lamellae over longer distances than in the case of the not yet sulfonated films. It seems that the sulfonation affects not only the bulk amorphous regions, but the inter-lamellar amorphous regions too, which has the consequence of swelling of lamellar stacks with an increase of the inter-lamellar spacing up to about L_D=180 Å. On the other hand, an isotropic halo is observed in the two-dimensional patters at intermediate Q (Fig. 6c), which gives rise to occurrence of the Guinier like size level that is clearly observed in the scattering pattern on equatorial sector (Fig. 5). Although apparently slightly deformed on meridian sector due to the presence of the strong inter-lamellar peaks (Fig. 6c), this halo can be considered isotropically distributed on the two-dimensional pattern and may be ascribed to the occurrence of a separate mesoscale morphology as a consequence of sulfonation. This may be a sort of spherical cluster-like morphology appearing due to the agglomeration of sulfonic groups, which changes the SLD of the amorphous region over a region of a characteristic size that is indicated by the Guinier regime.

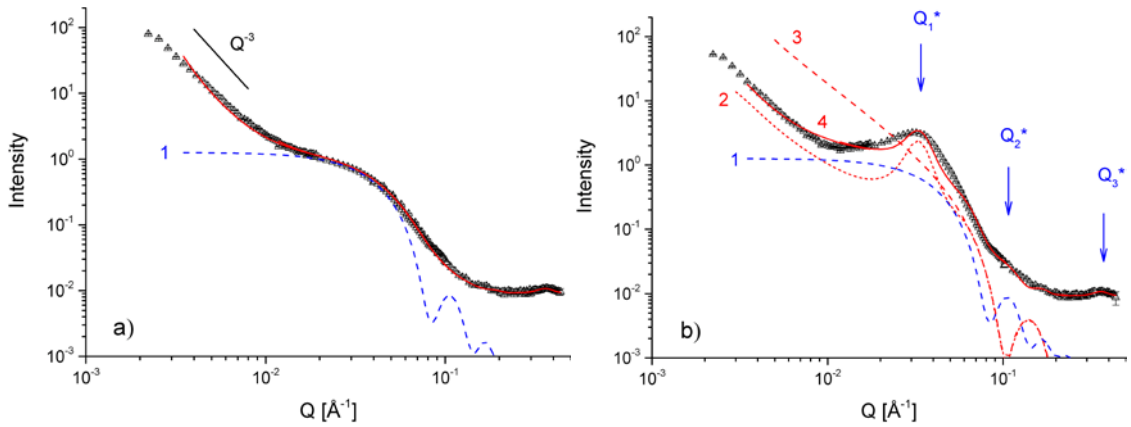

Fig. 7 – One-dimensional SANS pattern from a uni-axially deformed film clathrate with h-Tol and sulfonated obtained from the data averaging on equatorial sectors (a) and meridian sectors (b).The symbols indicate the experimentally measured data, while the lines indicate the model curves as following: full line (line 4 in panel b) – the overall fit of the experimental data, including the gaussian fit of the high-Q peak (Q_3* feature); dashed blue line (1) – the fitted spherical form-factor of the spherical cluster-like morphology (Eq. 4); dotted red line (2) – the fitted scattering contribution from the lamellar stacks (combining form-factor and structure-factor, Eqs. 5-6); dashed red line (3) - the fitted scattering contribution from the lamellae, Eq. 5 (neglecting the structure factor effect from the arrangement in stacks, Eq. 6).

Thus, in the complex structure yielded by the sulfonation of the clathrate sPS films two distinct morphologies could be identified. One is that of a spherical cluster-like local agglomeration of sulfonic groups, which is randomly distributed in the bulk amorphous region and produces a variation in SLD that yields the isotropic scattering hallo observed in Fig. 6c. Another morphology is that of the lamellar stacks oriented along the deformation direction, which give rise to the peaks observed in the meridian sectors in Figs. 6b and 6c. The averaging of the scattered intensity over the equatorial sectors will enable the characterization of the spherical cluster-like morphology, while over the meridian sector a superposition of two scattering contribution should be considered, namely from the spherical cluster-like morphology and from the oriented lamellar stacks.

Loading of the crystalline lamellae with different isotopologues as the guest molecules changes the contrast between the crystalline lamellae and amorphous regions, as reported elsewhere [59, 60]. Table 2 presents the calculated SLDs of the components in the investigated films. The results in Fig. 5 confirm that the presence of deuterated guest molecules in the clathrates yields a larger contrast between the crystalline and amorphous regions than the case with hydrogenated guest molecules. This is caused on one hand by the change of the scattering length density of the amorphous regions due to sulfonation compared to the neat state. On the other hand, protonated guests in crystalline lamellae decrease the scattering length density of the crystalline region, thus the contrast between sulfonated amorphous and clathrate crystalline regions. In contrast, deuterated guests in the lamellar region yield a higher contrast with the amorphous domains.

The data on the equatorial sector can be interpreted via the spherical form factor [78]

$$I_e(Q) = I_0^{sph}\left[3\frac{\sin(QR)-QR\cos(QR)}{(QR)^3}\right]^2 + Bckgd \qquad (4)$$

I_0^{sph} is the so-called "forward scattering" from the ensemble of spherical objects, which is proportional to the number density of spherical scattering objects, the volume squared of the spherical objects and the contrast factor squared between the scattering objects and the environment. *R* is the radius of the spherical scattering objects and *Bckgd* represents a constant background, which typically is observed towards high Q and is produced by the incoherent scattering from the sample. Fig. 7 presents the results of the fit of the intensity over the equatorial sector by Eq. 4, where the free parameters were considered as the radius *R* and the forward scattering (I_0^{sph}).

On the other hand, the major scattering contribution on the meridian sector that is produced by the oriented lamellar stacks superposes that from the cluster-like morphologies. Considering the form factor of an ensemble of lamellae dispersed in a sample volume [79, 80] the scattered intensity is given by

$$I(Q) = I_0^{lam}P(Q) = I_0^{lam}\left[\frac{\sin\left(\frac{Qd}{2}\right)}{\left(\frac{Qd}{2}\right)}\right]^2 \frac{D\left(\frac{QR_l}{2}\right)}{\left(\frac{QR_l}{2}\right)}(\pi R_l^2)^2 + Bckgd \qquad (5)$$

where I_0^{lam} is the forward scattering from the lamellae, d and R_l are the thickness and the lateral size of the lamellae and the Dawson function $D(u)$ exhibits the following asymptotic behavior: for $u \to \infty$, $2D(u)/u \to 1/u^2$ and for $u \to 0$, $D(u)/u \to 1$. When stacks of lamellae are formed, as in the case of semi-crystalline polymers, a structure factor arising from the interlamellar interference $S(Q)$ has to be multiplied by the single platelet form factor $P(Q)$ and the scattered intensity is defined by $I(Q) \approx P(Q)\, S(Q) + Bckgd$. For an ensemble of randomly oriented lamellar stacks the scattering pattern would be a sequence of rings, while for uni-axially oriented lamellar stacks along a specific direction clear peaks are observed in the scattering pattern, as depicted in Fig. 1. Considering a random variation in the distance of neighboring lamellae, the arising structure factor can be treated in terms of a one-dimensional paracrystalline structure [81]:

$$S(Q) = \frac{\sinh\left(Q^2\sigma_D^2/4\right)}{\cosh\left(Q^2\sigma_D^2/4\right) - \cos\left(QL_D\right)} \tag{6}$$

where L_D is the inter-lamellar distance and σ_D its dispersity. In a one-dimensional paracrystalline lattice, distortions of the second kind are considered, which means that the position of a lattice point only depends on the nearest neighbor position. The fluctuations of lamellar separations are not correlated and the long-range order is destroyed. This results in a lower intensity and a broadening of higher order peaks in SANS curves. Melt-drawn high-density polyethylene lamellar morphologies have been successfully characterized using the paracrystalline structure factor proposed by Hosemann [81, 82] combined with the form factor of a rectangular density profile [83].

Fig. 7 presents also the result of the fitting of the meridian data using the superposition of a contribution from the isotropic spherical cluster-like morphology and a contribution from the oriented lamellar stacks, as it is described above. The parameters characterizing the spherical cluster-like morphology (the radius R and the forward scattering I_0^{sph}) were considered fixed, as determined from the fit of the equatorial data. The free parameters were the thickness (d) and the forward scattering (I_0^{lam}) of the correlated lamellae together with the inter-lamellar distance (L_D) and its dispersity (σ_D). Infinitely large lamellae in the lateral direction were considered, as long as the lateral size of the lamellae should be outside the range of lengths covered by the experiment.

A Q^{-3} power law was considered in both the meridian and the equatorial cases at low Q. The instrument resolution was taken into account and the polydispersity of the spherical size (R) and lamellar thickness (d) were considered. It can be observed that the experimental curves are pretty well described by the fitted model curves which delivered a size of the spherical cluster-like morphology of R=55 Å and a lamellar thickness of d=62 Å with an inter-lamellar distance of about L_D=180 Å characterized by a dispersity of σ_D=54 Å. Both spherical clusters and lamellae are polydisperse in size (15%). The data interpretation in terms of these models also revealed the nature of the Q_2^* scattering feature: it seems that the hump observed in Fig. 4 and Fig. 5 at around $Q \cong 0.1$ Å^{-1} can be ascribed to a high-Q form factor detail that is smeared out by the size polydispersity of different morphologies and the instrumental resolution.

Finally, the peak-like feature Q_3* observed in all patters and high Q was included in the fit procedure as a Gaussian function that delivered the peak position and its width.

One should note here that the scattering pattern obtained after the averaging of data on meridian sectors (Fig. 7b) can be described by other functions, like for example a spherical form factor with an appropriate three-dimensional structure factor described by the hard-sphere model. Nevertheless, following the combined analysis of the observations done by SANS, WAXS and FTIR on clathrated and clathrated/sulfonated films the presence of the crystalline lamellae oriented and correlated over distances L_D's is certain and the peaks observed in the meridian sectors can be ascribed to inter-lamellar correlations between the oriented lamellae. Similar large inter-lamellar correlations, up to 200 Å, were observed in combined SAXS/WAXS investigations on different crystalline phases of different semi-crystalline polymeric systems [83-85].

3.3. SANS on hydrated films

Hydration of films drastically changes the two-dimensional scattering patterns. Fig. 8 shows in parallel the results from a dry and hydrated s-sPS film either with D_2O or H_2O. The film was initially clathrate with h-Tol. The inter-lamellar peak that was clearly observed in the pattern from the dry film disappears from the meridian sector due to hydration while another strong "butterfly like" scattering feature appears along equatorial sector. In contrast, no qualitative change between scattering patterns in the two states of hydration could be observed. Variation of the H_2O/D_2O ratio in hydrating water or of the H/D type of guest molecule in the clathrates do not change qualitatively the scattering patterns as well, but only affects the intensity level due to monotonous variation of the contrast between the amorphous and crystalline regions of the sample.

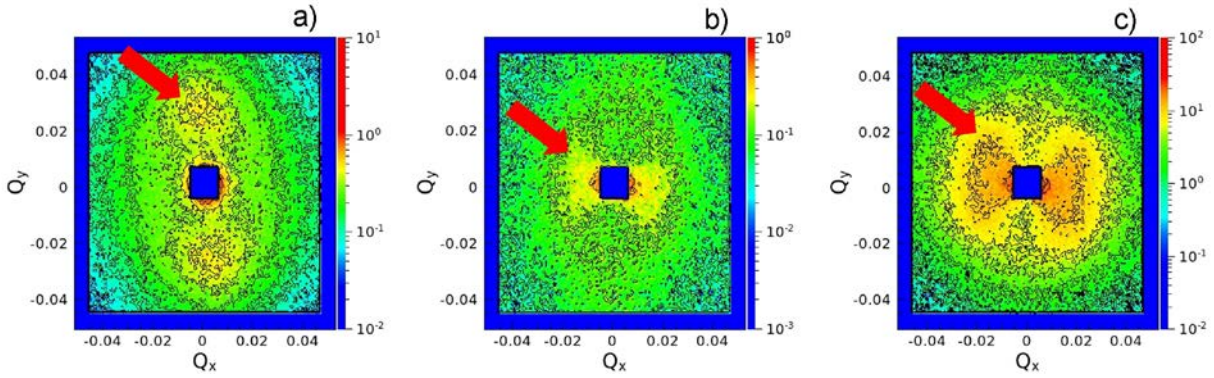

Fig. 8 – Two-dimensional scattering patterns from a s-sPS film (a) which was hydrated by dipping in D_2O (b) and, after drying, in H_2O (c); the red arrows indicate the main structural features: the peaks due to the inter-lamellar correlation in the meridian sectors in the case of the dry film and the "butterfly like" pattern in the equatorial sectors in the case of hydrated films.

In order to check the distribution of water molecules within the inter-lamellar and bulk amorphous regions we carried out SANS investigations on samples exposed to variable RH by using the humidity cell. In this setup the samples were placed in beam with the deformation axis horizontally, due to the geometry enabled by the sample holder. Therefore, all scattering features appear rotated with 90° compared to the cases presented in Figs. 6-8. First, a guest free s-sPS film (γ-phase) was tested. In Fig. 9 the scattering patterns collected on dry and hydrated γ-phase s-sPS system is presented for two different contrast conditions, provided by using either H_2O or D_2O.

Data analyzed on equatorial and meridian directions are shown in parallel. Snapshots of 1 minute were acquired in this case. The sample hydration from the dry state to 75% RH was completed in ca. 5 minutes, as estimated from the observed saturation of the intensity. The peak intensity increases or decreases compared to the dry state, as depending whether one uses H_2O or D_2O, as expected from the variation of the contrast between the crystalline and hydrated amorphous regions. The peak position does not change with the variation of the contrast. This would be indicative for water accumulation mostly in the bulk amorphous region, out of the lamellar stacks. Water accumulates in the inter-lamellar amorphous region only scarcely, hence no observed swelling of the inter-lamellar layers, thus of changes in the peak position.

The intensity behavior averaged over the meridian sector (oppositely to the peak one) resembles that in Fig. 5 and indicates the formation of an additional morphology. Interestingly, in the D_2O hydration state the intensity behaves like Q^{-1}, which would indicate the presence of one-dimensional morphologies that are evidenced by this special contrast condition.

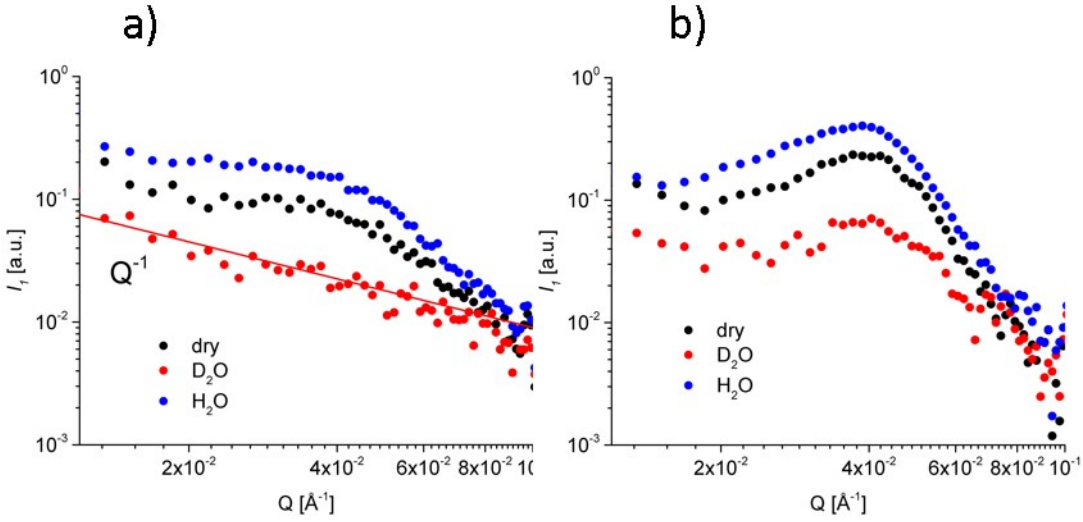

Fig. 9 – One-dimensional SANS patterns from a s-sPS uni-axially deformed film in γ phase which was exposed to D_2O and H_2O vapors using the humidity chamber at RH=75%. The left panel presents data averaged over a direction perpendicular to the deformation axis while the right panel shows the data averaged in the inter-lamellar peak sectors.

A selection of the SANS measurements performed on a δ-phase s-sPS film exposed to different humidity generated with H_2O is presented in Fig. 10. The sample was first subjected to a gradual

increase in humidity from RH=10% to RH=95% and was subsequently dried back to RH=10%. The results depict in detail the morphological changes occurring in the sample as a consequence of hydration and drying effect. Up to RH=80% a gradual increase in the intensity from the inter-lamellar peaks is observed in the equatorial direction while the peak position does not change. The intensity increase is a consequence of the increase in contrast due to water accumulation in the amorphous regions. At a humidity of RH=85% (Fig. 10c) each peak seems to split into 2 peaks which migrate away from the equatorial line. At RH=95% four diagonally positioned peaks are clearly revealed.

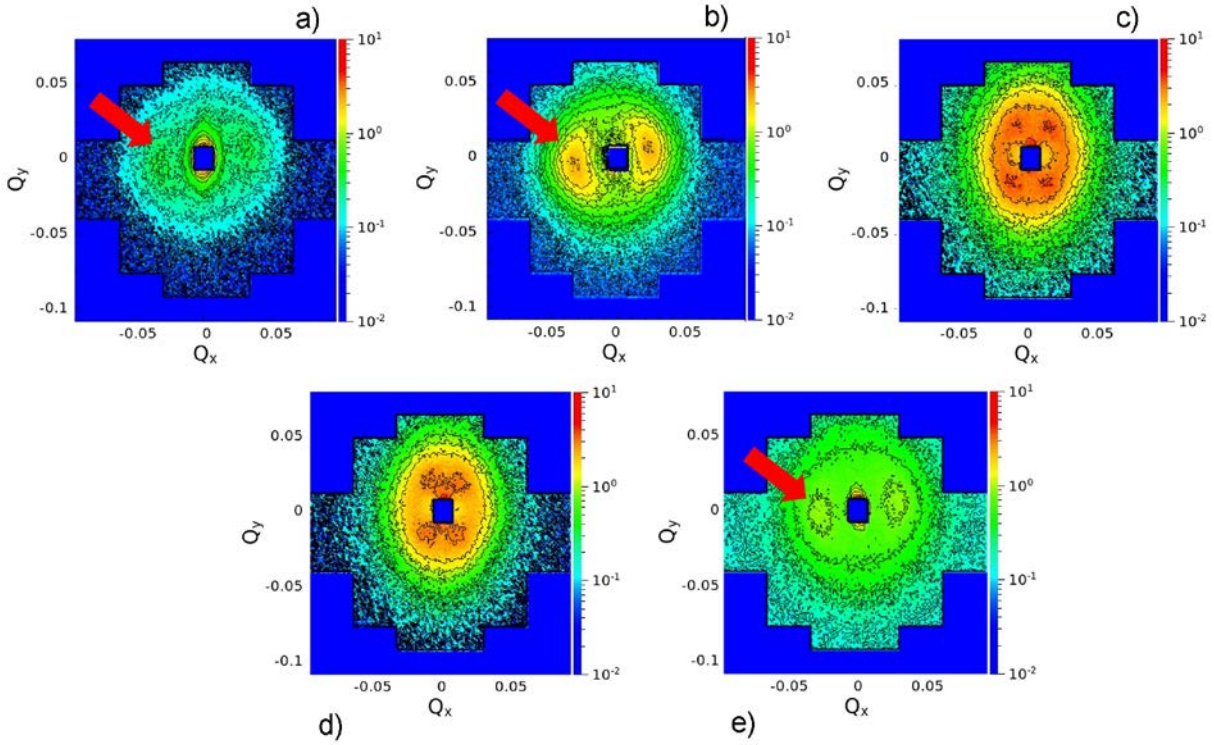

Fig. 10 – Two-dimensional SANS patterns from an s-sPS film (clathrate with h-Tol) exposed to H_2O vapors in a humidity cell. The RH values are like following: a) 10%, b) 50%, c) 85%, d) 95% and e) 10% again. The RH on the sample was varied in a controlled way in both wetting and drying directions.

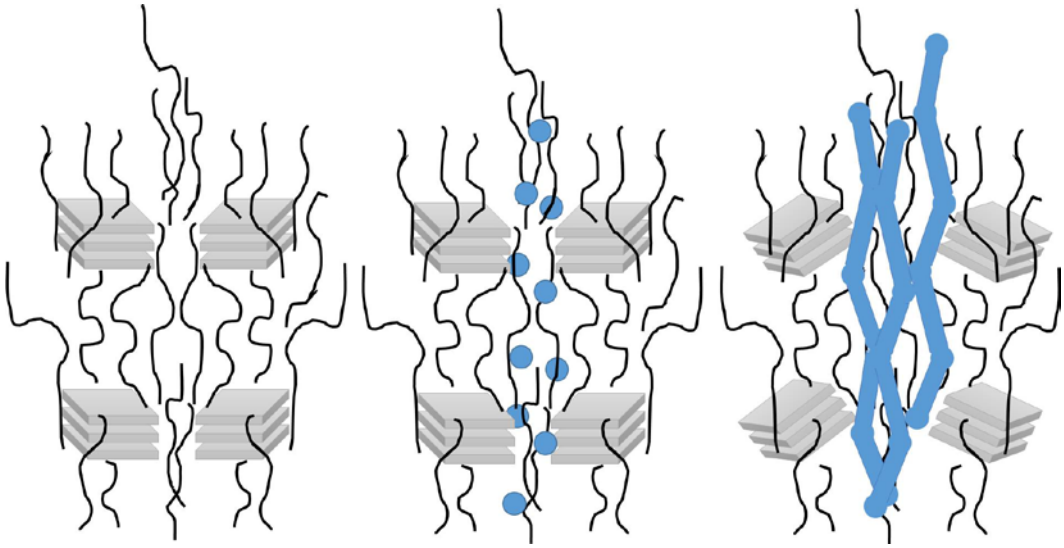

Fig.11 – Schematic view of the morphological changes occurring in s-sPS clathrate films exposed to a gradual increase of humidity as derived from the qualitative interpretation of the SANS data. At low and moderate humidity water clusters are formed in the bulk amorphous region while at high humidity (RH>85%) water channels are formed which induce a displacement and inclination of the lamellar stacks.

The scattering features in Fig. 10d resemble the well-known "butterfly like" or 4-spots patterns previously observed in SAXS and SANS investigations of deformed semi-crystalline polymers or rubbers [86]. After drying the sample back to RH=10% the initial scattering pattern was recovered. This proves that the behavior of the deformed dry s-sPS film when it is exposed to a humid atmosphere resembles that of a semi-crystalline polymer or elastomer under deformation.

The occurrence of the 4-spots pattern at RH=95% can be ascribed to internal deformations and stress induced by water accumulation in the bulk amorphous region. Initially, in the dry state, the stacks of parallel and vertically correlated lamellae are aligned in parallel direction with the uni-axially film deformation. Water uptake by the s-sPS film seems to form initially domains that grow inside the bulk amorphous regions. Then upon increasing the RH further the crystalline lamellar stacks move away from their initial almost parallel orientation towards an inclined orientation. Upon drying the film the water domains vanish and the deformation and stress against the lamellar stacks ceases, enabling the initial orientation and position to be recovered. The proposed mechanism for explaining this behavior is depicted in Fig. 11.

This process may explain also why no structural change was observed in the two-dimensional scattering patterns (Fig. 8) regardless of the deuteration/protonation degree of hydration water. With the water accumulated only scarcely between the lamellae, the contrast between the crystalline lamellae and the inter-lamellar amorphous regions suffers only minor changes. Thus the 4-spot pattern remains always visible. Unlike this, the contrast between the lamellar stacks and the bulk amorphous regions changes when water is up-taken. Hence, the variation of the peak intensity between the deuterated and protonated hydration states in Fig. 9.

Fig. 12 shows the one-dimensional scattering data from a sample hydrated with H_2O at different RH. The data were averaged in sectors along the perpendicular direction to the deformation axis (Fig. 12a) and over the peak sectors (Fig. 12b). Data collected over a wide Q range are shown. A gradual change in position of the high-Q peak is observed with gradually increasing RH. The peak moves towards low Q values, which reveals the nature of the peak: this is the "ionomer peak" which originates from the hydrophobic-hydrophilic nanophase separation in the polymer film. Its position depends on the level of film hydration [87]. The swelling behavior can be discussed in terms of the dilution law, which is determined from the plot $d_{max} = f(\phi_p)$, where ϕ_p is the polymer volume fraction and $d_{max} = 2\pi/Q_3^*$, where Q_3^* is the ionomer peak position [88, 89]. The polymer volume fraction can be roughly estimated from the interpretation of the "forward scattering" from the hydrated domains in Fig. 12a (determined in a similar manner as the fit of the equatorial scattering pattern in Fig. 7) in terms of the scattering contrast squared from the common polymer-water morphologies embedded in an amorphous polymer matrix, in which the polymer volume fraction in the common morphologies will appear also as ϕ_p^2. Fig. 13 present the obtained dilution law with a -1/3 exponent. Typically, the lamellar systems obey a dilution law with an exponent -1, the rod-like systems – an exponent of -1/2 while the spherical particles – an exponents of -1/3.

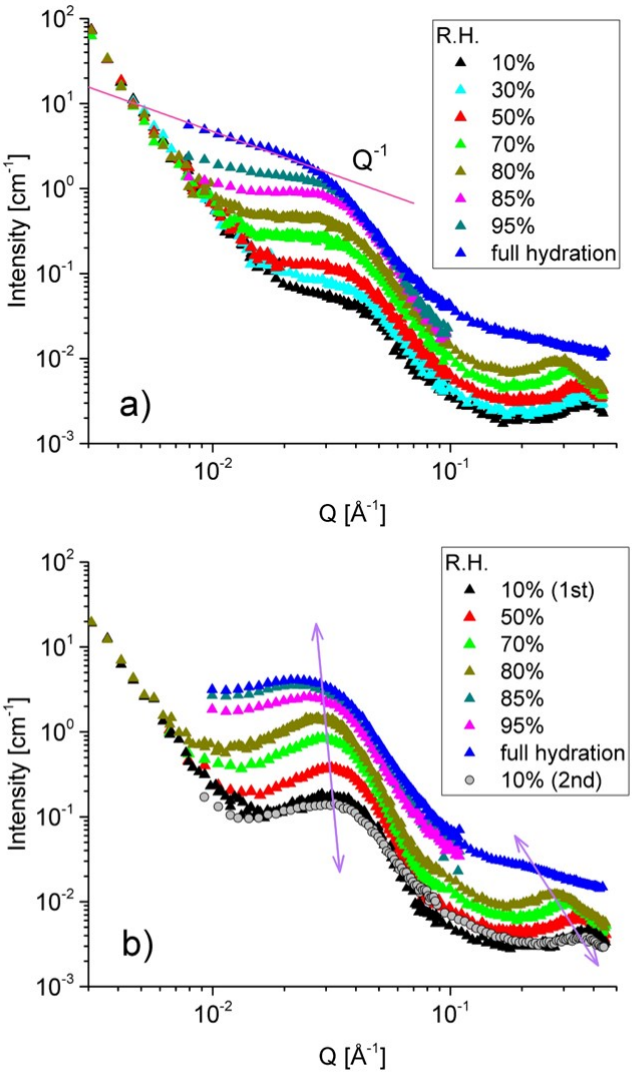

Fig. 12 – One-dimensional SANS patterns from an s-sPS film (clathrate with h-Tol) exposed to H_2O humidity for different values of RH and fully hydrated (by dipping in H_2O). The panel a) present the data averaged over the sectors perpendicular to the deformation direction while in the panel b) data averaged over the peak sectors (see Fig. 12) are shown.

Fig. 12a shows that a special morphology grows at the mesoscale upon increasing the RH, as indicated by the evolution of the scattering profile at intermediate Q. The scattering patterns resemble that from small spherical morphologies at low and moderate RH while at high RH the Q^{-1} intensity behavior proves formation of a one-dimensional long morphology. This possibly evolves from the smaller morphologies formed in lower RH conditions. The intensity from the one-dimensional morphologies drops too steep towards high Q to be attributed to a form factor effect from ideal cylindrical structures. Similar scattering patterns were observed in the case of the polymer rods with density modulation along the rod axis [80] or the polymer necklace morphology [90]. Correlation effects along the one-dimensional morphologies in these cases

yield broad-like humps in the Q-region where the intensity deviates from the Q^{-1} behavior, which can be observed also in the scattering profile from the full hydrated sample in Fig. 12a.

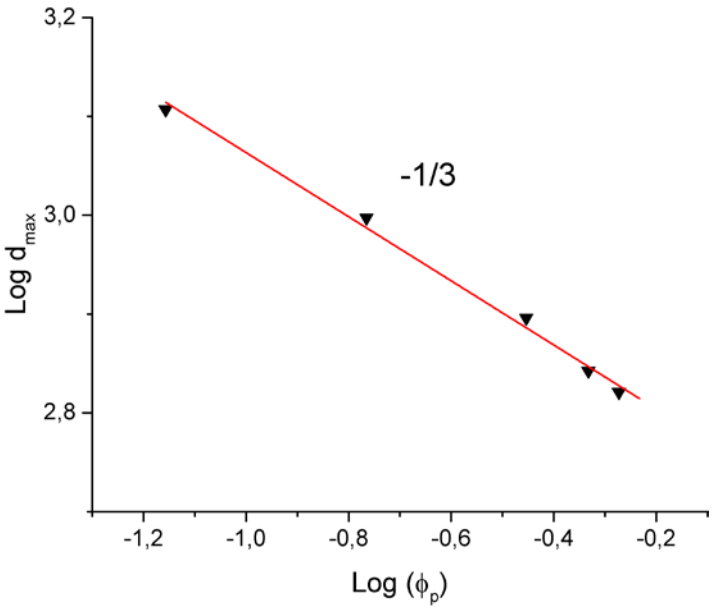

Figure 13 – Evolution of the ionomer peak as a function of the polymer volume fraction during hydration of the s-sPS film for different values of RH.

The scattering profiles averaged over the sectors of the inter-lamellar peak show that the change in peak position with humidity variation is almost indistinguishable. This confirms the findings in Fig. 9. By drying the sample the inter-lamellar peak recovers exactly the same position and profile as before the hydration. These observations indicate that hydration is affecting only marginally the lamellar stacks. Moreover, they prove the mechanical strength of such films, which is conferred by their crystalline regions.

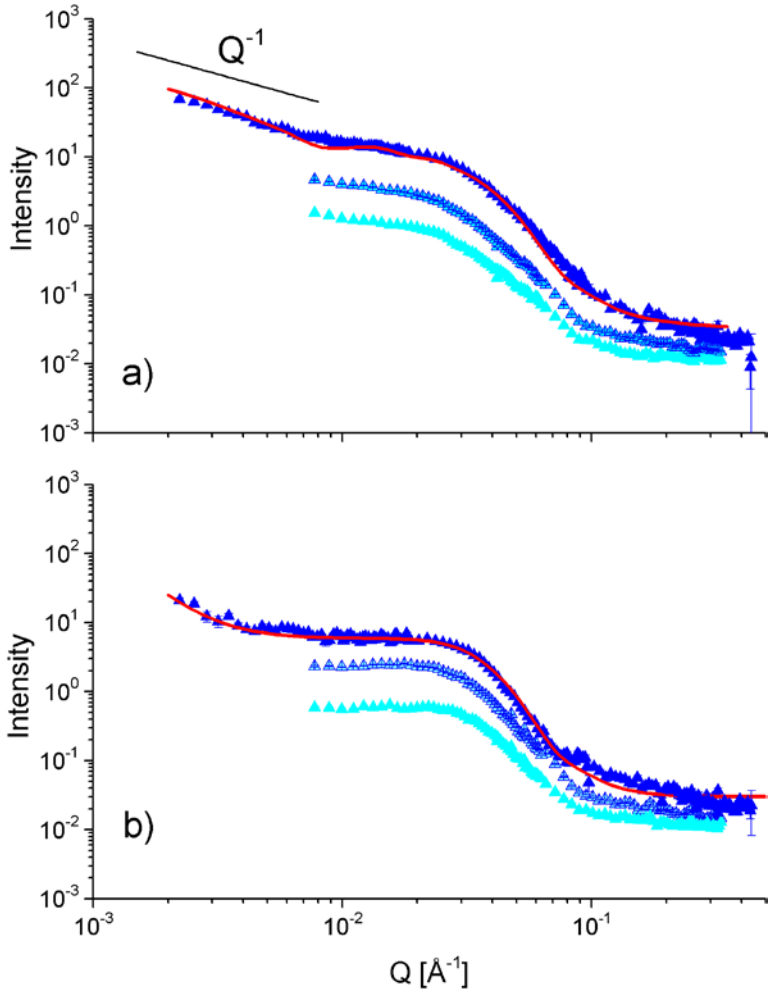

743

744 Fig. 14 - One-dimensional SANS patterns in the equatorial (a) and meridian (b) sectors (sample
745 geometry like Fig. 1) from s-sPS films fully hydrated by dipping in D_2O/H_2O mixtures with 0%, 30%
746 and 70% D_2O volume fraction (from the upper to the lower curve in each panel). In red are the model
747 curves that describe the experimental data according to the necklace model [86].

748

749 With the three main features Q_1^*, Q_2^* and Q_3^* explained, we tried a characterization of the
750 morphologies in the amorphous region – responsible for the water transport in the film – as a
751 function of contrast variation based on dipping of the s-sPS film in D_2O/H_2O mixtures of
752 different compositions and the measuring the films in the fully hydrated state. Fig.14 shows the
753 scattering patterns averaged over the meridian and equatorial sectors, thus none of theseare the
754 inter-lamellar peak sector. Variation of the H_2O/D_2O ratio in the hydrating water does not
755 change qualitatively the scattering patterns, but only affects the intensity level. The meridian
756 sector data show a typical spherical form factor behavior with a steep decay towards high Q,
757 which may be indicative of weak correlation effects. The scattering patterns in the equatorial
758 sectors are characterized by a higher intensity level than those in the meridian sector and by a
759 different qualitative behavior. The main feature is the broad hump at intermediate Q which
760 evolves towards low Q in a Q^{-1} power law pattern. The power law behavior is indicative of long
761 one-dimensional morphologies, as already revealed in Fig. 12a.

762

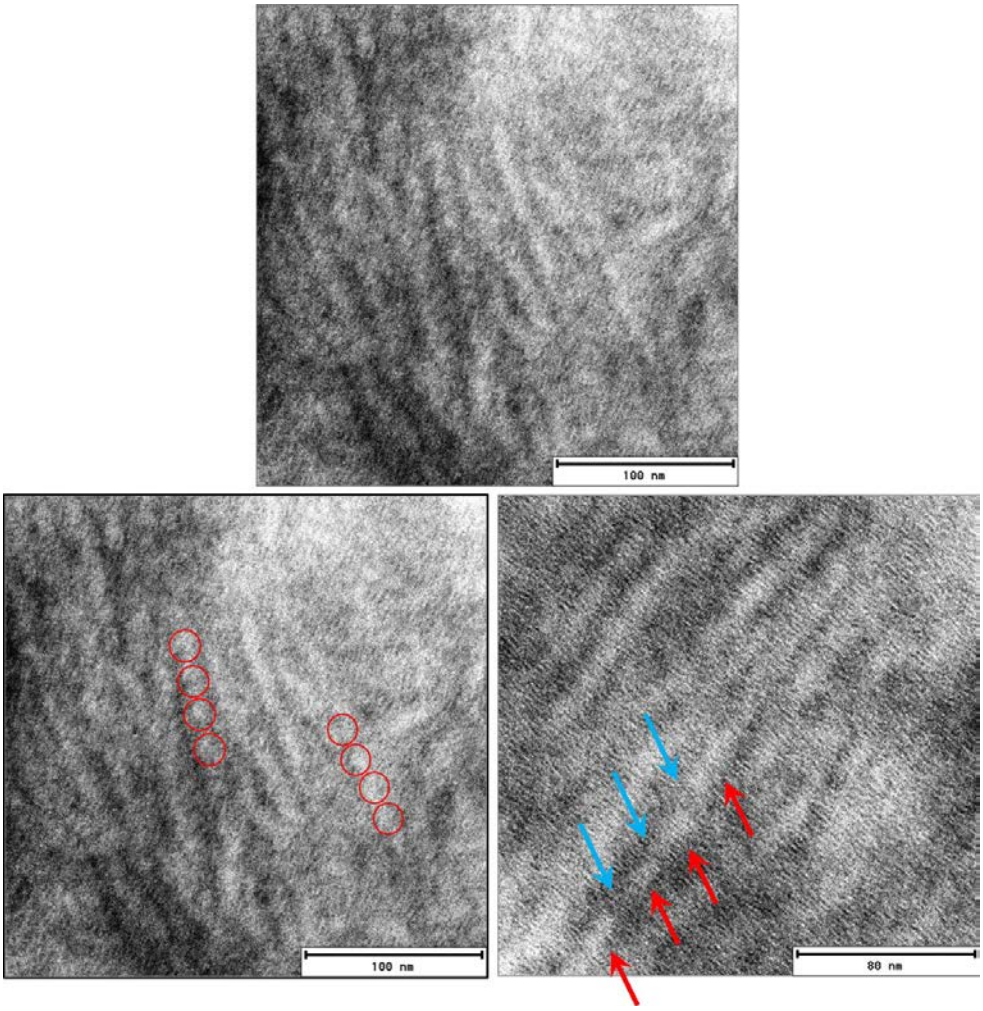

763

764 Fig. 15 – TEM micrograph from a hydrated s-sPS uni-axially deformed film captured by using the cryo
765 option. Oriented one-dimensional morphologies of alternating variable thickness (indicated by the red
766 and blue arrows) along the main axis are observed. The thicker sections of the morphology (indicated
767 by the red arrows) resemble an ensemble of spherical beads (clusters).

768

769 The qualitative interpretation of the SANS results suggests a one-dimensional morphology with
770 spherical clusters distributed along the main axis that are formed due to the hydration of the
771 amorphous regions in the s-sPS films, as presented in Fig.11. The cryo-TEM observation
772 supports this idea as displayed in Fig. 15. One-dimensional morphologies with variable
773 thickness within the range 100-150 Å can be observed. These morphologies are oriented along
774 the direction of the uni-axial deformation applied to the films. Also, they present a longitudinal
775 profile that resembles a thickness modulation along the main axis.

776 Based on SANS and cryo-TEM results we propose a potential scenario for the hydration
777 mechanism to produce a morphology like shown in Fig. 11. We suspect that water is taken-up
778 at low RH in spherical clusters, which form around the -SO_3H groups, favored by the increased
779 flexibility of the sPS chains in the bulk amorphous domains. The amorphous sPS segments in
780 the inter-lamellar regions are characterized by reduced flexibility. Therefore, clustering of -
781 SO_3H groups and growth of water domains is much less favored in this region. With increasing

humidity, the clusters increase in number and eventually join together turning into a one-dimensional morphology like that sketched in Fig. 11, right panel. These are the morphologies with variable thickness that produce the scattering feature Q^{-1} and are revealed by cryo-TEM. This scenario support the findings by SANS.

With the correlation peaks migrating out of the meridian sector (or, the equatorial one in the case of using the humidity cell) the data in the meridian and equatorial sectors in the fully hydrated state would reflect only the morphological behavior of the amorphous regions. The ensemble of vertically oriented cylinders should give rise to appearance of specific scattering features in the equatorial sector, which will correspond to correlation effects between cylinders. No detail about a correlation effect other than that between the crystalline lamellae can be clearly seen in the two-dimensional scattering pattern. The modeling of the scattering from aligned cylindrical channels was reported in [91] while the necklace model (beads connected by narrower strings) is presented in detail in [90, 92]. To combine these models in order to characterize such a complex morphology like that proposed in the model sketch for the fully hydrated state is a very complicated procedure. We attempted to check how the SANS data from such a morphology (Fig. 14, lines) could be modeled to get reliable structural parameters using a more simple approach based only on the necklace model. The fit was done using the simple spherical form factor with weak correlation structure factor added [86] for the scattering pattern in meridian sector while for the equatorial sector the necklace form factor was used [90]. Both models describe well the experimental data for a size of the spherical cluster of about $R_{cluster}$=70 Å. While the necklace model evidenced a correlation effect over a length of about $L_{cluster}$=490 Å between a number of clusters that form a linear arrangement, which is longer than the largest size observed in the Q-window of the SANS investigation. This correlation length is obviously too large for the inter-cluster spacing that can be estimated from the cryo-TEM pictures. We believe that the approach we used is too simple to accurately describe the complex morphology and, therefore, we can only speculate that such a long-range correlation could actually represent a weak correlation effect between the oriented cylinders.

Conclusions

Deuterated syndiotactic polystyrene (sPS) films have been produced by casting or drawing and uniaxial deformation. The films have been partially crystallized (clathrate) by dipping in different solvents. Sulfonated-sPS (s-sPS) was produced by the furthermore treatment of the films in a chloroform-based acyl sulfate solution. The sulfonation affected only the amorphous regions of films. Subsequent guest exchange provided the embedding of specific guest molecules, either deuterated or protonated toluene, in the crystalline regions. Subsequently, the films were hydrated through dipping or exposure to water vapors using a humidity chamber that provided a controlled relative humidity (RH) on the sample. The films were characterized after each step of the complex preparation – clathration, functionalization with -SO_3H, guest exchange, hydration and drying – by FTIR, WAXD and SANS under different contrast conditions provided by manipulating the deuteration/protonation degree of either the guest molecule in the crystalline regions or the hydration water taken-up by the amorphous domains. SANS on uni-axially deformed films at different degrees of RH helped to understand the

complex morphology shown by the films. The sPS contains crystalline and amorphous regions. The crystalline regions consist of lamellar stacks of crystalline lamellae that contain guest molecules, which alternate with inter-lamellar amorphous regions. The sulfonation functionalizes the sPS in both the bulk and inter-lamellar amorphous regions. Hydration affects mostly the bulk amorphous regions. Water is taken-up at low RH in clusters formed around the $-SO_3H$ groups, favored by the increased flexibility of the sPS chains in the bulk amorphous domains. At high RH the water clusters in the bulk amorphous regions become interconnected one with another and a cylindrical morphology is formed. Observations made by cryo-TEM of fully hydrated films supports the SANS conclusions. Previously, s-sPS has been demonstrated as good candidate for PEM in fuel-cell applications. We characterized in detail the microscopic environment that supports the high conductivity exhibited by this material, comparable to that of Nafion.

TABLE 1: Characteristics of the s-sPS films after the sulfonation and hydration procedures.

Parameter	**Stretched Sample**	**Un-stretched Sample**
S content (%)	13.6	10.5
S / C ratio	0.181	0.135
Sulfonation degree (%)	54.2	40.4
IEC	2.14	1.23
$W_{up\text{-}take}$ (%)	120	51
$W_{content}$ (%)	55	33
$\lambda = [H_2O]/[SO_3\text{-}]$ (number of water molecules per ion exchange site)	31	23

TABLE 2. Neutron scattering length density of different compounds in the samples.

Compound	**SLD [*10^{10} cm^{-2}]**	**Mass density [g cm^{-3}]** reference [24]
sPS crystalline	6.47	0.977
sPS amorphous	6.00	1.051
-SO_3H	1.10	
D_2O	6.34	
H_2O	-0.56	
d-Tol	5.66	
h-Tol	0.94	

Acknowledgements

We would like to thank Prof. C. De Rosa and Prof. F. Auriemma for the permission to use the WAXS diffractometer of the University Federico II of Naples.

References

[1]. Kreuer K.D., *J. Membr. Sci.* **2001**, 185 (1), 29−39.

[2]. Li B., Wang L.D., Kang B.N., Wang P., Qiu Y., *Sol. Energy Mater. Sol. Cells* **2006**, 90 (5), 549−573.

[3]. Geise G.M., Freeman B.D., Paul D.R., *Polymer* **2010**, 51 (24), 5815−5822.

[4]. Smitha B., Sridhar S., Khan A.A., *Journal of Membrane Science* **2005**, 259, 10-26.

[5]. Larminie J., Dicks A., *Fuell Cell Systems Explained, 2nd Edition*, John Wiley & Sons, **2003**.

[6]. Hickner M.A., Ghassemi H., Kim Y.S., Einsla B.R., McGrath J.E., *Chem. Rev*. **2004**, 104, 4587-4611.

[7]. Rikukawa M., Sanui K., *Prog. Polym. Sci.* **2000**, 25, 1463-1502.

[8]. Hamrock S.J., Yandrasits M.A., *Polym. Rev*. **2006**, 46, 219-244.

[9]. Peckham T.J., Holdcroft S., *Adv. Mater.*, **2010**, 22, 4667.

[10]. Park M. J., Kim S.Y., *Journal of Polymer Science Part B: Polymer Physics* **2013**, 51, 481.

[11]. Borriello A., Lavorgna M., Malagnino N., Mensitieri G., Napolitano T., Nicolais L., *Macromol. Symp*. **2004**, 218, 293.

[12]. Napolitano T., Coffa S., Mensitieri G., Borriello A., Nicolais L., EP 1494307B1, **2006**.

[13]. Lavorgna M., Fusco, L.,Piscitelli, F., Mensitieri, G., Agoretti, P., Boriello, A., Mascia, L., *Pol. Eng. Sci.* **2008**, 2398.
[14]. Fasano G., Califano, R., Pellegrino, M., Venditto, V., Guerra, G., Borriello, A., Ambrosio, L., Sansone, L., *Int. Journal. of Hydrogen Energy* **2013**, 36, 8038.
[15]. Schellenberg J., in *Syndiotactic Polystyrene*, John Wiley & Sons, Inc., **2010**.
[16]. Gowd E.B., Tashiro K., Ramesh C., *Progress in Polymer Science* **2009**, 34, 280.
[17]. Guerra G., Vitagliano V., De Rosa C., Petraccone V., Corradini P., *Macromolecules* **1990**, 23 (5), 1539.
[18]. De Rosa C., Guerra G., Petraccone V., Corradini P., *Polymer Journal (Tokio, Japan)* **1991**, 23 (12), 1435.
[19]. Chatani Y., Shimane Y., Ijitsu T., Yukinari T., *Polymer* **1993**, 34 (8), 1625.
[20]. Cartier L., Okihara T., Lotz B., *Macromolecules*, **1998**, 31 (10), 3303.
[21]. Auriemma F., Petraccone V., Dal Poggetto F., De Rosa C., Guerra G., Manfredi C., Corradini P., *Macromolecules* **1993**, 26 (15), 3772.
[22]. Tashiro K., Ueno Y., Yoshioka A., Kobayashi M., *Macromolecules* **2001**, 34 (2), 310.
[23]. Rizzo P., Albunia A.R., Guerra G., *Polymer* **2005**, 46, 9549.
[24]. De Rosa C., Guerra G., Petraccone V., Pirozzi B., *Macromolecules* **1997**, 30, 4147.
[25]. Milano G., Venditto V., Guerra G., Cavallo L., Ciambelli P., Sannino D., *Chem. Mater.* **2001**, 13, 1506.
[26]. Rizzo P., Daniel C., De Girolamo Del Mauro A., Guerra G., *Chem. Mater.* **2007**, 19, 3864.
[27]. Rizzo P., D'Aniello C., De Girolamo Del Mauro A., Guerra G., *Macromolecules* **2007**, 40, 9470.
[28]. Petraccone V., Ruiz O., Tarallo O., Rizzo P., Guerra G., *Chem. Mater.* **2008**, 20, 3663.
[29]. Tarallo O., Petraccone V., *Macromol. Chem. Phys.* **2004**, 205, 1351.
[30]. Tarallo O., Petraccone V., *Macromol. Chem. Phys.* **2005**, 206, 672.
[31]. Petraccone V., Tarallo O., Venditto V., Guerra G., *Macromolecules* **2005**, 38, 6965.
[32]. Tarallo O., Petraccone V., Venditto V., Guerra G., *Polymer* **2006**, 47, 2402.
[33]. Guerra G., Daniel C., Rizzo P., Tarallo O., *Journal of Polymer Science Part B: Polymer Physics* **2012**, 50, 305.
[34]. Uda Y., Kaneko F., Tanigaki N., Kawaguchi T., *Adv. Mater.* **2005**, 17, 1846.
[35]. Kaneko F., Uda Y., Kajiwara A., Tanigaki N., *Makrom. Chem. Rapid. Commun.* **2006**, 27, 1643.
[36]. Zinck P., Bonnet F., Mortreux A., Visseaux M., *Progress in Polymer Science* **2009**, 34, 369.
[37]. Jaymand M., *Polym. Chem.*, **2014** DOI:10.1039/c3py01551c.
[38]. Orler E. B., Yontz D. J., Moore R. B., *Macromolecules*, **1993** 26, 5157.
[39]. Li H. M., Liu J. C., Zhu F. M., Lin S. A., *Polym. Int.*, **2001**, 50, 421.
[40]. Scherer G. G., *Ber. Bunsen-Ges. Phys. Chem.*, **1990**, 94, 1008.
[41]. Büchi F. N., Buvanesh G., Haas O., Scherer G. G., *Electrochemica Acta*, **1995**, 40, 345.
[42]. Guo Q., Pintauro P. N., Tang H., O'Connor S., *J. Member. Sci.*, **1999**, 154, 175.
[43]. Saga S., Matsumoto H., Saito K., Minagawa M., Tanioka A., *J. Power Sources*, **2008**, 176, 16.
[44]. Raut P., Liang W., Chen Y-M., Zhu Y., Jana S. C., *ACS Appl. Mater Interfaces*, **2017**, 9, 30933.
[45]. Gierke, T. D., Munn, G. E., Wilson, F. C., *J. Polym. Sci. Polym. Phys. Edn* **1981**, 19, 1687.

[46]. Dreyfus, B., Gebel, G., Aldebert, P., Pineri, M. & Escoubes, M., *J. Phys. France* **1990**, 51, 1341.
[47]. Gebel, G. & Lambard, J., *Macromolecules* **1997**, 30, 7914.
[48]. Jang, S. S., Molinero, V., Cagin, T., Goddard III, W. A., *Solid State Ion.* **2004**, 175, 805.
[49]. Haubold, H.-G., Vad, T., Jungbluth, H., Hiller, P., *Electrochim. Acta* **2001**, 46, 1559.
[50]. Litt, M. H., *Polym. Preprint* **1997**, 38, 80.
[51]. Kreuer, K. D. *J. Membr. Sci.* **2001**, 185, 29.
[52]. Kim, M.-H., Glinka, C. J., Grot, S. A. & Grot,W. G., *Macromolecules* **2006**, 39, 4775.
[53]. Rollet, A.-L., Diat, O., Gebel, G., *J. Phys. Chem. B* **2002**, 21, 3033.
[54]. Rubatat, L., Rollet, A.-L., Gebel, G., Diat, O. *Macromolecules* **2002**, 35, 4050.
[55]. Rubatat, L., Gebel, G., Diat, O. *Macromolecules* **2004**, 37, 7772.
[56]. Schmidt-Rohr, K., Chen, Q., *Nature Materials* **2008**, 7, 75.
[57]. Kreuer, K. D., Portale, G., *Adv. Funct. Mater.* **2013**, 23, 5390.
[58]. Kusoglu, A., Weber, A. Z., *Chem. Rev.* **2017**, 117, 987.
[59]. Kaneko, F., Radulescu, A., Ute, K., *Polymer* **2013**, 54, 3145.
[60]. Kaneko, F., Radulescu, A., Ute, K., *J. Appl. Cryst.* **2014**, 47, 6.
[61]. Borriello A., Agoretti P., Ambrosio L. Fasano G., Pellegrino M., Venditto V., Guerra G., *Chem. Mater.* **2009**, 21, 3191-3196.
[62]. Gromadzki D., Černoch P., Janata M., Kůdela V., Nallet F., Diat O., Štěpánek P., *European Polymer Journal* **2006**, 42, 2486-2496.
[63]. Revay, Z., *Journal of large-scale research facilities* **2015**, 1, A20.
[64]. Zhou, L., Roddecha, S., Anthamatten, M., *Polymer* **2009**, 50, 3136.
[65]. Schneider, C.A., Rasband, W.S., Eliceiri, K.W., *Nature Methods* **2012**, 9, 671.
[66]. Radulescu, A., Szekely, N., Appavou, M-S., Pipich, V., Kohnke, T., Ossovyi, V., Staringer, S., Schneider, G. J., Amann, M., Zhang-Haagen, B., Brandl, G., Drochner, M., Engels, R., Hanslik, R., Kemmerling, G., *J. Vis. Exp.* **2016**, 118, e54639.
[67]. Li H.-M., Liu J.-C., Zhu F.-M., Lin S.-A., *Polymer International* **2001**, 50, 421.
[68]. Martins C.R., Ruggeri G., De Paoli M.-A., *J. Braz. Chem. Soc.* **2003**, 14, 797.
[69]. Todorovskii A.T., Plotkin S. Ya., *Zhurnal Prikladnoi Spektroskopii,* **1989**, 51, 597.
[70]. Castagna A.M., Wang W., Winey K.I., Runt J., *Macromolecules,* **2010**, 43, 10498.
[71]. Zhou N.C., Burghardt W.R., Winey K.I., *Macromolecules,* **2007**, 40, 6401.
[72]. Revay Z., *Anal. Chem.*, **2009**, 81, 6851.
[73]. Albunia, A. R., D'Aniello C., Guerra G., *Cryst. Eng. Comm.*, **2010**, 12, 3942.
[74]. Gebel, G., Diat, O., *Fuel Cells* **2005**, 5, 261.
[75]. Mendil-Jakani, H., Zamanillo Lopez, I., Legrand, P. M., Mareau, V. H., Gonon, L., *Phys. Chem. Chme. Phys.* **2014**, 16, 11228.
[76]. Beaucage, G., *J. Appl. Cryst.*, **1996**, 29, 134.
[77]. Strobl, G. R., Schneider, M., *J. Pol. Sci.: Pol. Phys. Ed.* **1980,** 18, 1343.
[78]. Pedersen, J. S., *Adv. Colloid Interface Sci.*, **1997**, 70, 171.
[79]. Richter, D., Schneiders, D., Monkenbusch, M., Willner, L., Fetters, L. J., Huang, J. S., Lin, M., Mortensen, K., Farago, B., *Macromolecules,* **1997**, 30, 1053.
[80]. Radulescu, A., Fetters, L. J., Richter, D., *Adv. Pol. Sci.* **2008**, 210, 1.
[81]. Hosemann, R., Bachi, S. N., *Direct Analysis of Diffraction by Matter*, North-Holland: Amsterdam, 1962.
[82]. Hosemann, R., Loboda-Cackovic, J., *J. Polymer Sci.*, **1975**, 53, 159.
[83]. Fischer, S., Jiang, Z., Men, Y., *J. Phys. Chem. B,* **2011**, 115, 13803.

963 [84]. Tashiro, K. in *Electroactive Polymers (EAP),* Materials Research Society, Warrendale,
964 Pensylvania, **2000**.
965 [85]. Bhoje Gowd, E., Shibayama, N, Tashiro, K., *Macromolecules* **2008**, 41, 2541.
966 [86]. Pakula, T., Saijo, K., Kawai, H., Hashimoto, T., *Macromolecules* **1985**,18, 1294.
967 [87]. Fumagalli, M.m Lyonnard, S., Prajapati, G., Berrod, Q., Porcar, L., Guillermo, A.,
968 Gebel, G., *J. Phys. Chem. B* **2015**, 119, 7068.
969 [88]. Gebel, G., *Macromolecules* **2013**, 46, 6057.
970 [89]. Berrod, Q., Lyonnard, S., Guillermo, A., Ollivier, J., Frick, B., Manseri, A., Ameduri,
971 B., Gebel, G., *Macromolecules* **2015**, 48, 6166.
972 [90]. Schweins, R., Huber, K., *Macromol. Symp.* **2004**, 211, 25.
973 [91]. Marchal, D., Deme, B., *J. Appl. Cryst*. **2003**, 36, 713.
974 [92]. Dobrynin, A. V., Rubinstein, M., Obukhov, S. P., *Macromolecules* **1996**, 29, 2974.